Wavelet Transforms and Ocean Current Data Analysis

PAUL C. LIU AND GERALD S. MILLER

Great Lakes Environmental Research Laboratory, NOAA, Ann Arbor, Michigan*

(Manuscript received 31 July 1995, in final form 26 March 1996)

ABSTRACT

The recently advanced approach of wavelet transforms is applied to the analysis of ocean currents. The conventional analyses of time series in the frequency domain can be readily generalized to the frequency and time domain using wavelet transforms. An application of wavelet analysis to a set of observed current data acquired during the spring of 1991 in Lake Michigan shows some significant time-localized characteristics that would not be detected using the traditional Fourier transform approach.

1. Introduction

Fourier spectrum analysis has been used in the analysis of Eulerian current meter observations since power spectrum analysis was introduced to oceanic studies. With the further introduction of fast Fourier transform algorithms and increased availability of new instruments for measuring currents, spectrum analysis has continued to be one of the standard procedures used for analyzing observed current data.

Fourier spectrum analysis generally provides frequency information about the energy content of observed time series data. This information, however, pertains only to the time span of the observational data and its proper interpretation presumed that the data is stationary. Changes and variations within a time series cannot be easily unraveled. Stationarity in the data simply represents a statistical idealization. Its validity is usually regarded as an approximation of the field condition. The effectiveness of applying Fourier spectrum analysis to a rapidly changing current field, such as during frontal crossing or rapidly changing wind fields, is questionable. The emergence of wavelet transform analysis, which can yield localized time-frequency information without requiring that the time series be stationary, has presented a promising complementary approach to the traditional Fourier spectrum analysis, and has provided significant new perspectives for the analysis of Eulerian current measurements. An exploratory attempt to adopt the versatile wavelet transform analysis to analyze an interesting episode of current measurements during a spring atmospheric frontal passage in Lake Michigan during 1991 is presented in this paper.

2. Wavelet transform and rotary spectra

Following a standard formulation (Combes et al. 1989), we briefly summarize the wavelet transform. Starting with a family of functions, the so-called analyzing wavelets, $\psi_{s\tau}(t)$, that are generated by dilations s, and translations τ, from a mother wavelet $\psi(t)$, as

$$\psi_{s\tau}(t) = \frac{1}{|s|^{1/2}}\psi\left(\frac{t-\tau}{s}\right), \tag{1}$$

where $s \neq 0$, $-\infty < \tau < +\infty$. The continuous wavelet transform of a time series $X(t)$ is then defined as the inner product of $\psi_{s\tau}$ and X as

$$\tilde{X}(s,\tau) = \langle \psi_{s\tau}, X \rangle = \frac{1}{|s|^{1/2}}\int_{-\infty}^{+\infty} X(t)\psi^*\left(\frac{t-\tau}{s}\right)dt, \tag{2}$$

or equivalently in terms of their corresponding Fourier transforms

$$\tilde{X}(s,\tau) = |s|^{1/2}\int_{-\infty}^{+\infty} \hat{X}(\omega)\hat{\psi}^*(s\omega)e^{i\tau\omega}d\omega, \tag{3}$$

where an asterisk superscript indicates the complex conjugate. In essence, the wavelet transform takes a one-dimensional function of time into a two-dimensional function of time τ and scale s (or equivalently, frequency).

The function to be used as a choice of mother wavelet $\psi(t)$ can be either real or complex valued. But in order for the wavelet transformation to be invertible, it needs to satisfy the *admissibility condition*

* GLERL Contribution Number 966.

Corresponding author address: Dr. Paul C. Liu, Great Lakes Environmental Research Laboratory, NOAA, 2205 Commonwealth Blvd., Ann Arbor, MI 48105-1593.
E-mail: Liu@glerl.noaa.gov

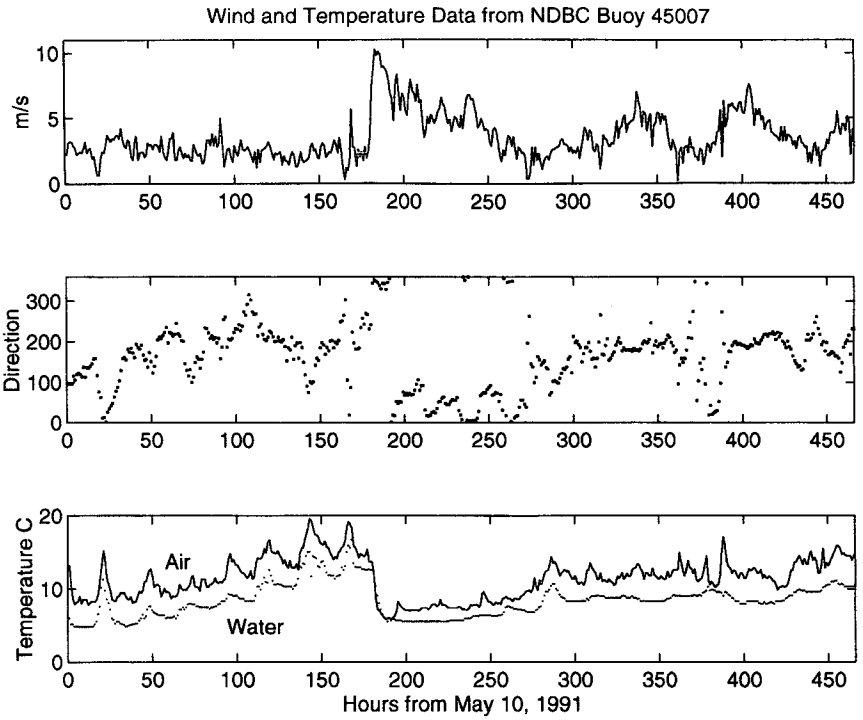

FIG. 1. Plots of wind speed, wind direction, air temperature, and water temperatures recorded by NDBC buoy 45007 during 10–30 May 1991.

$$\int_{-\infty}^{+\infty} \frac{|\hat{\psi}(\omega)|^2}{\omega} d\omega < \infty, \tag{4}$$

which is equivalent to

$$\hat{\psi}(0) = \int_{-\infty}^{+\infty} \psi(t) dt = 0. \tag{5}$$

Thus, $\psi(t)$ should have zero mean with oscillations that decay at infinity.

Now, regarding $X(t)$ as the current velocity vector, it can be written in the form of a complex time function as

$$X(t) = u(t) + iv(t), \tag{6}$$

where $u(t)$ and $v(t)$ are, respectively, the east–west and north–south scalar components of the current measurements. Their corresponding Fourier transforms are

$$\hat{X}(\omega) = \hat{u}(\omega) + i\hat{v}(\omega), \tag{7}$$

where $\hat{u}(\omega)$ and $\hat{v}(\omega)$ are Fourier transforms of $u(t)$ and $v(t)$, respectively. From (3) we can also have the corresponding wavelet transforms as

$$\tilde{X}(s, \tau) = \tilde{u}(s, \tau) + i\tilde{v}(s, \tau). \tag{8}$$

Here $\tilde{u}(s, \tau)$ and $\tilde{v}(s, \tau)$ are wavelet transforms of $u(t)$ and $v(t)$, respectively. In analogy with Fourier energy density spectrum analysis, we can readily obtain the wavelet spectrum (Liu 1994) for current vector data as

$$\tilde{X}(s, \tau)\tilde{X}^*(s, \tau) = \tilde{u}(s, \tau)\tilde{u}^*(s, \tau) + \tilde{v}(s, \tau)\tilde{v}^*(s, \tau), \tag{9}$$

or

$$|\tilde{X}(s, \tau)|^2 = |\tilde{u}(s, \tau)|^2 + |\tilde{v}(s, \tau)|^2. \tag{10}$$

A frequently used approach of current data analysis is to resolve the velocity vector into two rotational components—clockwise and counterclockwise (Mooers 1973; Gonella 1972). [A useful summary of these techniques is given by Konyaev (1990).] Analogous to the Fourier analysis approach, we can convert the scales into frequency and represent the wavelet transform of current velocity $\tilde{X}(\omega, t)$ in the time-frequency space as the sum of the clockwise U_- and counterclockwise U_+ components. Thus, at each frequency at a given time, there are two rotating vectors. The vector with positive frequency rotates counterclockwise, and the vector with negative frequency rotates clockwise as

$$U_+(\omega, t) = |U_+(\omega, t)|\exp[-i\theta_+(\omega, t)], \quad \omega \geq 0 \tag{11}$$

and

$$U_-(\omega, t) = |U_-(\omega, t)|\exp[i\theta_-(\omega, t)], \quad \omega < 0, \tag{12}$$

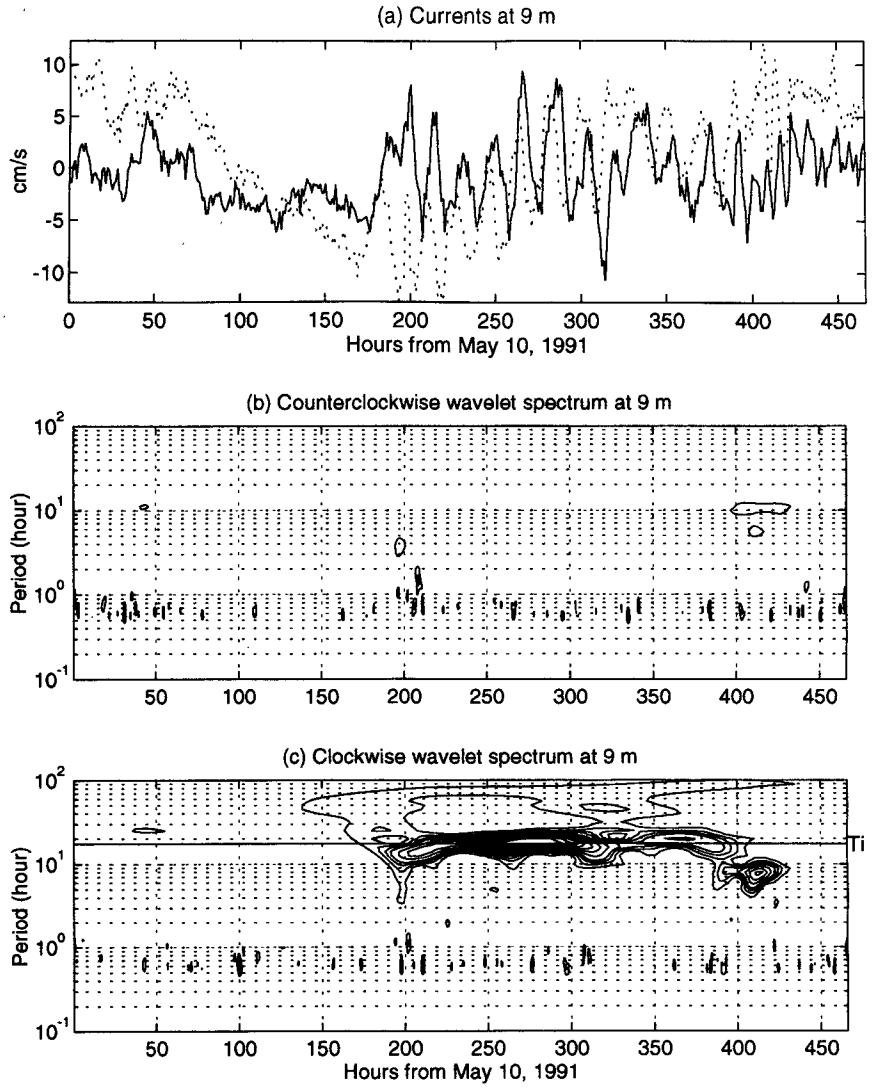

FIG. 2. (a) Current measurement at 9 m below the water surface. The top panel shows the time series data of the two components of the current velocity [solid line for $u(t)$ and dashed line for $v(t)$]. (b) and (c) Contour plots of the counterclockwise and clockwise components, respectively, of the wavelet spectrum of the current velocity. The theoretical inertial period is marked as Ti with a corresponding line drawn across the panel.

where θ_+ and θ_- are the phase of the complex functions U_+ and U_-, respectively. If we further let the wavelet transforms of Cartesian components $\tilde{u}$ and $\tilde{v}$ be represented by their real and imaginary parts as

$$\tilde{u}(\omega, t) = \tilde{u}_r(\omega, t) + i\tilde{u}_i(\omega, t) \tag{13}$$

and

$$\tilde{v}(\omega, t) = \tilde{v}_r(\omega, t) + i\tilde{v}_i(\omega, t), \tag{14}$$

then by equating the wavelet transforms in terms of rotational components with that of Cartesian components and considering that the real and imaginary parts of $\tilde{u}$ and $\tilde{v}$ are even and odd, respectively, we have, for $\omega \geq 0$,

$$U_+(\omega, t) = \tilde{u}_r(\omega, t) - \tilde{v}_i(\omega, t) + i[\tilde{u}_i(\omega, t) + \tilde{v}_r(\omega, t)], \tag{15}$$

and for $\omega < 0$,

$$U_-(\omega, t) = \tilde{u}_r(\omega, t) + \tilde{v}_i(\omega, t) + i[\tilde{u}_i(\omega, t) - \tilde{v}_r(\omega, t)]. \tag{16}$$

Hence, the counterclockwise and clockwise wavelet

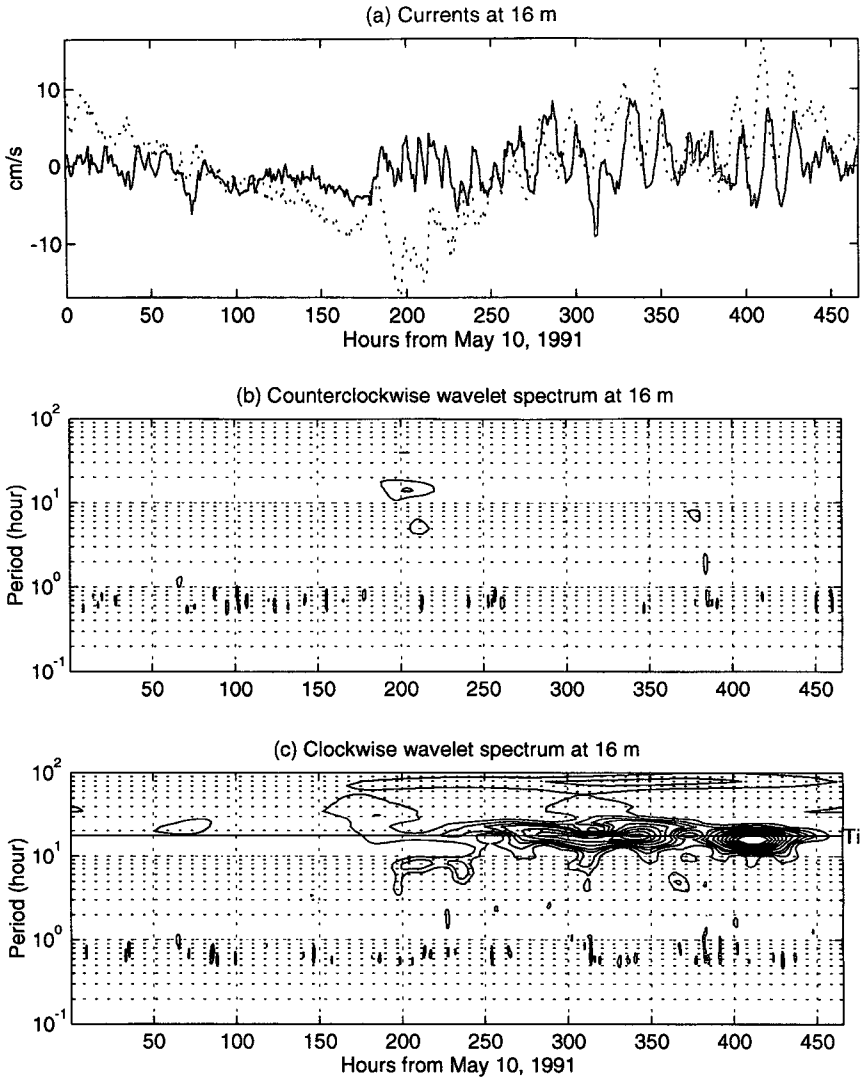

FIG. 3. Same as Fig. 2. Current measurement at 16 m below the water surface.

spectra can be readily obtained, respectively, in terms of the wavelet transforms of Cartesian components as

$$|U_+(\omega, t)|^2 = [\tilde{u}_r(\omega, t) - \tilde{v}_i(\omega, t)]^2 + [\tilde{u}_i(\omega, t) + \tilde{v}_r(\omega, t)]^2 \quad (17)$$

and

$$|U_-(\omega, t)|^2 = [\tilde{u}_r(\omega, t) + \tilde{v}_i(\omega, t)]^2 + [\tilde{u}_i(\omega, t) - \tilde{v}_r(\omega, t)]^2. \quad (18)$$

Thus, the conventional rotary current data analysis in the frequency domain using Fourier transforms can be directly extended to the time-frequency domain using wavelet transforms.

In the practical applications of wavelet transform, the choice of appropriate wavelet is generally based on the purpose of analysis (Farge 1992). In this study, we choose to use the complex-valued, modulated Gaussian wavelet known as the Morlet wavelet, readily available and widely used in studies of geophysical processes. This wavelet, originally proposed by Morlet et al. (1982), is given by

$$\psi(t) = (e^{imt} - e^{-m^2/2})e^{-t^2/2}. \quad (19)$$

Its Fourier transform is

$$\hat{\psi}(\omega) = (2\pi)^{1/2}[e^{-(\omega-m)^2/2} - e^{-m^2/2}e^{-\omega^2/2}], \quad (20)$$

where $m \geq 5$ is a constant parameter that renders the second term in (19) and (20) negligible. We follow Daubechies (1990) by adopting $m = \pi(2/\ln 2)^{1/2} = 5.336$ for our application in this study. For the calculation of Morlet wavelet transform in practice, a ger-

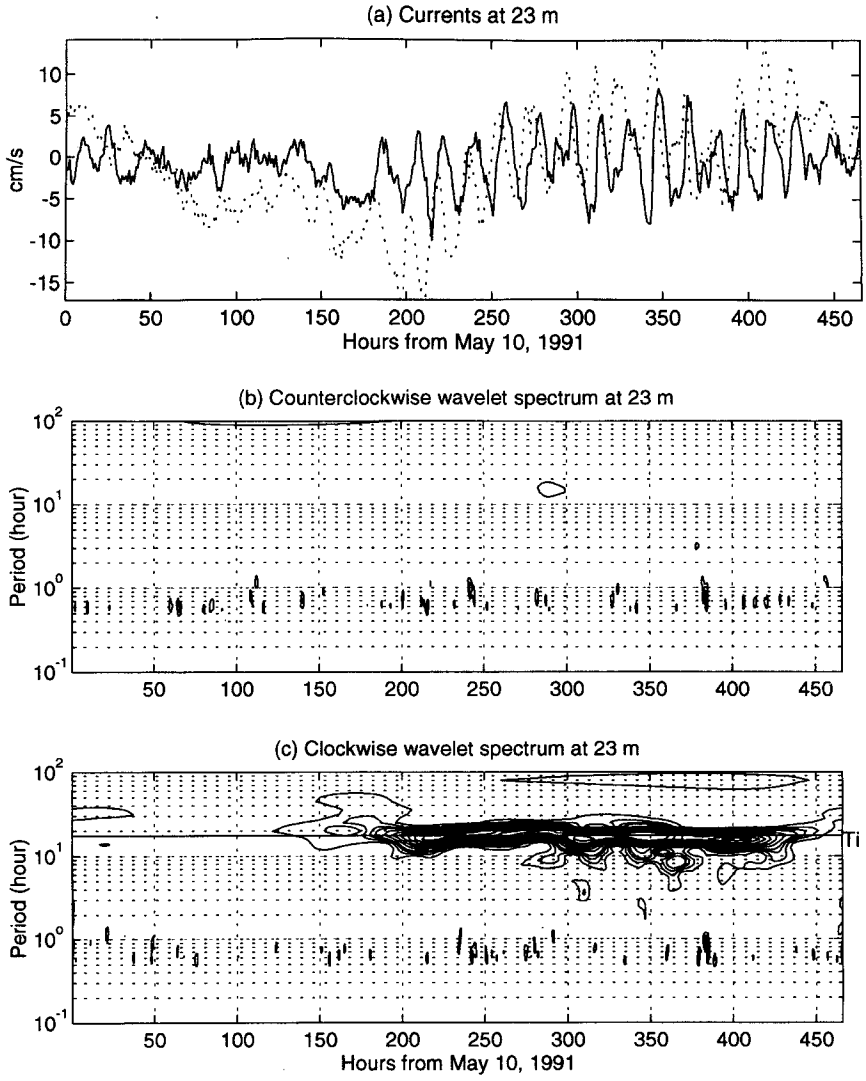

FIG. 4. Same as Fig. 2. Current measurement at 23 m below the water surface.

mane description of detailed procedures had been given in Weng and Lau (1994). Note that since $\hat{\psi}(0) \approx 0$ is true only in an approximate sense, the Morlet wavelet does not strictly satisfy the admissibility condition (5). However, as we are not concerned with data reconstruction here, Morlet wavelet with its advantageous property of stable frequency localizations is well suited for our studies.

3. Applications

As we have seen, wavelet transform analysis is a logical generalization of the widely used Fourier transform analysis for analyzing current vector data. Now we wish to show how wavelet transform analyses of current data can reveal characteristics of the current vector time series that would be difficult, if not impossible, to obtain from the usual Fourier transform. The current velocities used in this application were measured using a moored acoustic Doppler current profiler (ADCP) during a study of the vernal thermal front in Lake Michigan during the period of 10–30 May 1991 (Moll et al. 1993). The mooring was located 6.8 km off the eastern shore of Lake Michigan near Grand Haven, Michigan, in 41-m water depth. A National Data Buoy Center (NDBC) instrumented buoy (45007) in the center of southern Lake Michigan provided wind and temperature information. Figure 1 presents the time series of wind speed, wind direction, air temperature, and water temperature recorded from the buoy.

The 600-kHz upward-looking ADCP was programmed for 1-m depth cells and 15-min sampling rate. The current velocities selected for this study was measured at five levels: 9, 16, 23, 30, and 36 m below the

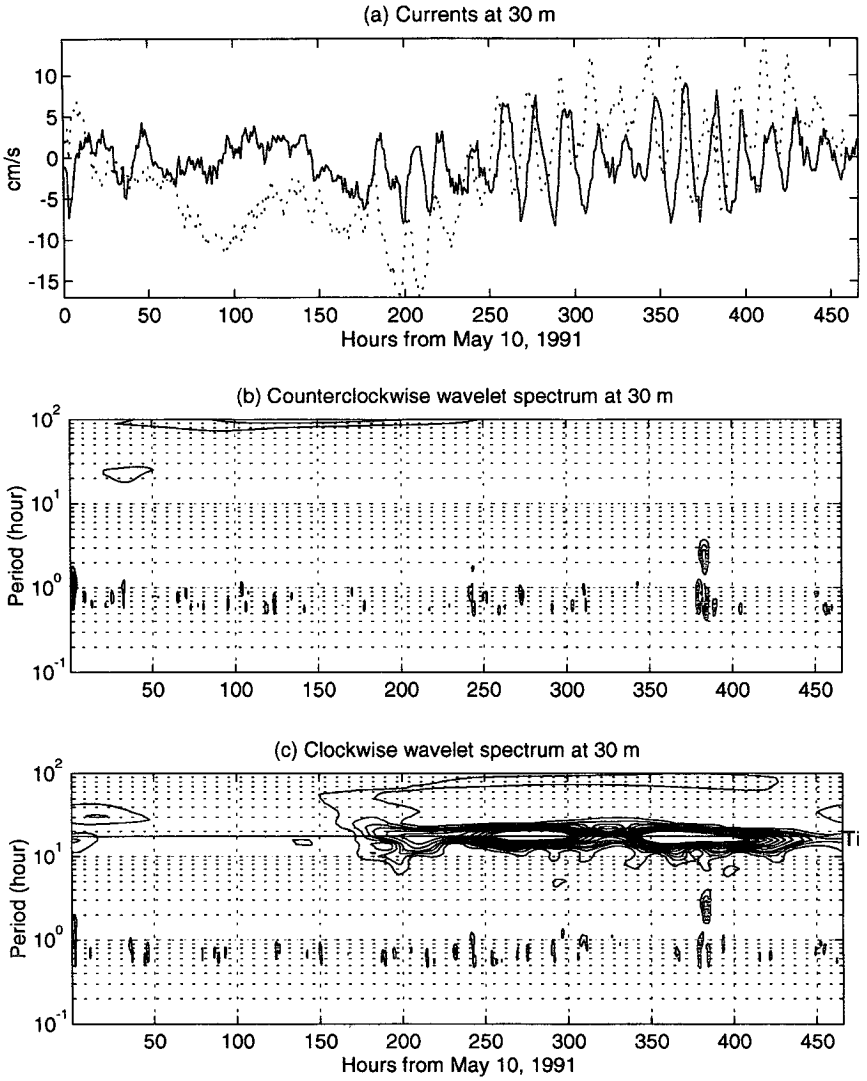

FIG. 5. Same as Fig. 2. Current measurement at 30 m below the water surface.

water surface. Plots of the east–west $u(t)$ and north–south $v(t)$ components of the measurements and contours of the calculated wavelet spectrum for the counterclockwise and clockwise components of the velocity field at the five levels are shown in Figs. 2–6. In these figures we have plotted the inverse of frequency (the period), for the convenience of periodicity visualization.

Examination of these figures shows some of the interesting aspects of this dataset. Lake Michigan, like other deep temperate lakes, undergoes a transition from isothermal, fully mixed in winter to thermally stratified in summer during the recording period. The onset of this transition appears to occur around 16 and 17 May and correlates with the passage of an atmospheric front where a northward wind field abruptly switched to southward with an increase in wind speed and a decrease in air and water temperatures (Fig. 1). The current field begins to exhibit vigorous periodic oscillations at all levels. The wavelet spectrum analysis of the current field clearly shows the onset time of energetic clockwise current oscillations at all levels at a period of approximately 17 h. The theoretical inertial period Ti shown by the solid line drawn across, is 17.58 h for this location. The lack of counterclockwise oscillations and strong dominance of clockwise rotating motions near the local inertial period is expected for summer lake conditions, which are characterized by a well-mixed upper layer separated from a cold lower layer by a sharp thermocline (Mortimer 1963, 1993).

In addition to the strong inertial oscillations, there are also noticeable oscillations at the low- and high-frequency ends of the wavelet rotary spectra shown

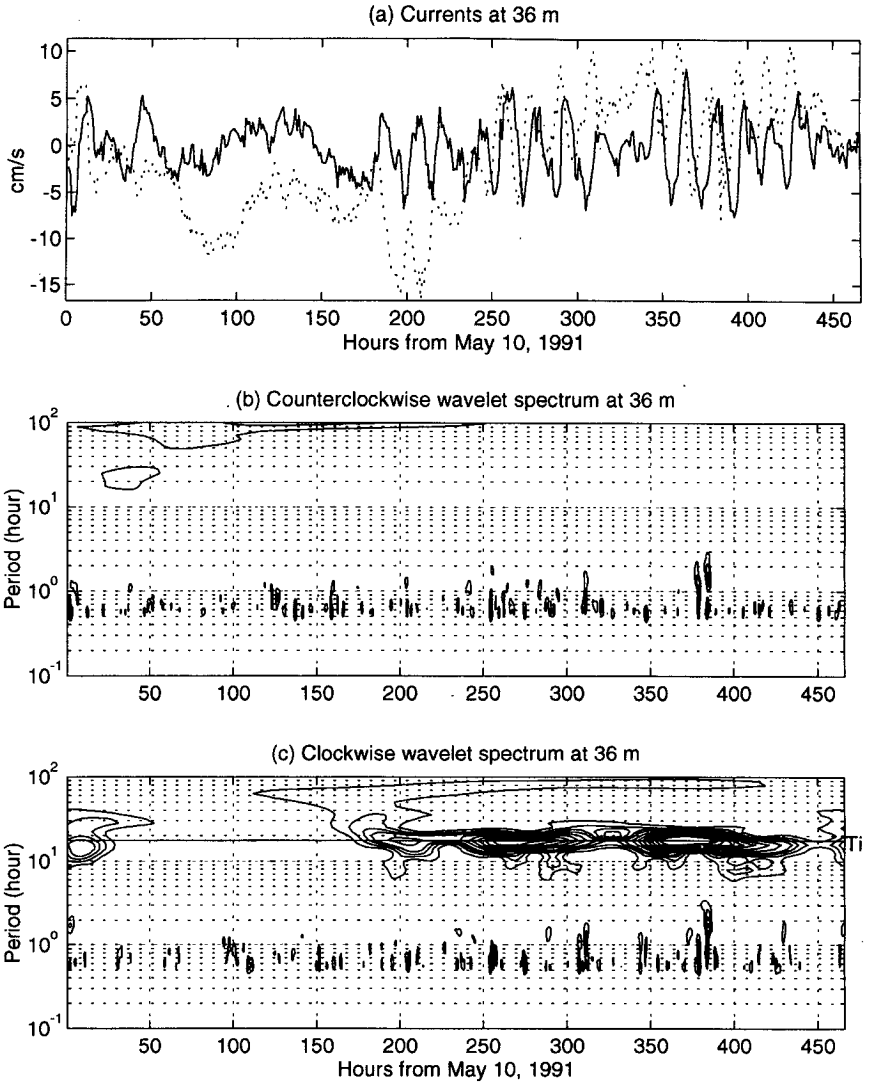

FIG. 6. Same as Fig. 2. Current measurement at 36 m below the water surface.

in Figs. 2–6. On the low-frequency side, a persistent oscillation of nearly 100 h in period appears in the clockwise wavelet spectra along with strong inertial oscillations at all levels. It appears also in the counterclockwise wavelet spectra but prior to the onset of strong inertial oscillations, especially at deeper levels. This 100-h oscillation has been identified by Saylor et al. (1980) as the lowest-order barotropic, vortex mode of southern Lake Michigan.

On the high-frequency side, there are also series of intermittent weak oscillations at slightly below 1-h period that appear in both the clockwise and counterclockwise cases at all levels. These oscillations have also been observed in the study of normal modes of Lake Michigan by Rao et al. (1976) but not theoretically identified. The wavelet spectrum of wind speeds (Fig. 7), recorded at NDBC buoy 45007 in the center of Lake Michigan during the same time, shows similar intermittent fluctuations at slightly below 1-h periodicities. As the wind speeds are only hourly data, it is uncertain if those high-frequency oscillations might be wind generated. However, the persistent and energetic process above 10-h period in the wavelet spectrum of wind speeds shown in Fig. 7, corresponding to the strong oscillations shown in Figs. 2–6, indicates that the near-inertial motions are basically wind driven.

While conventional rotary spectrum analysis using Fourier transforms generally identifies the clockwise oscillations at the inertial frequency in the data, the wavelet transform approach can further detect the specific time when the clockwise energy strengthened after the atmospheric frontal passage. However, it is of interest to note that an oscillation at twice the inertial frequency that has been observed previously using

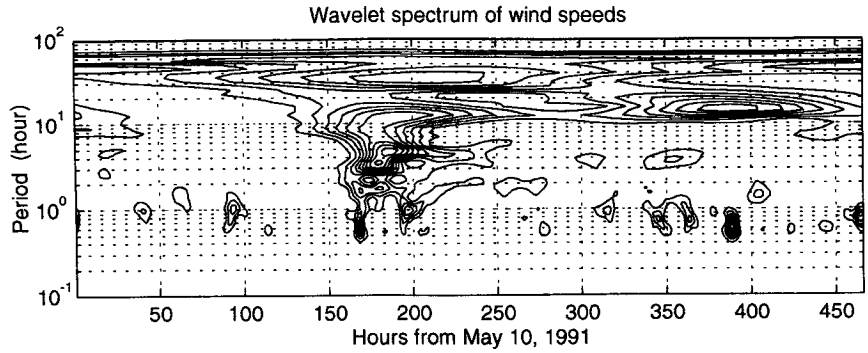

FIG. 7. Wavelet spectrum of wind speeds recorded by the NDBC buoy 45007.

Fourier spectrum analysis (Mortimer 1993) does not seem to be present in the wavelet spectra. To facilitate a direct comparison between wavelet and conventional approaches, Fig. 8 shows the plot of mean wavelet rotary spectra at 36-m level integrated and averaged over time. Figure 9 is a plot of conventional rotary spectra calculated using the fast Fourier transform (FFT) approach with hourly averaged data. The characteristics shown in Figs. 8 and 9 are generally similar. The wavelet results appear much smoother than the Fourier results, clearly the capability and flexibility of using a broad range of scale decompositions in wavelet transform is a distinctive advantage even for familiar spectral representation and applications.

A further interesting aspect that can be examined using the wavelet technique is to ascertain the direction of phase propagations. Leaman and Sanford (1975) analyzed the time series of vertical velocity profiles obtained with an electromagnetic velocity profiler during the international Mid-Ocean Dynamics Experiment and interpreted the resulting clockwise rotary spectrum as the evidence of downward energy propagation, which corresponds to upward phase propagation in the inertial waves. Direct observational evidence of this well-known feature does not seem to be explicitly available. In essence, upward propagation in phase should be readily visualized from simultaneous time series plots of either u or v component of currents at different levels. Figure 10 presents a time-series plot for resultant current speeds $[(u^2 + v^2)^{1/2}]$ during the intense period of inertial motions that shows manifestly the distinctive forward phase shift as the currents extended progressively upward.

This qualitative fact can now be demonstrated quantitatively using wavelet transforms. As the Morlet wavelet is complex, its wavelet transform extracts both amplitude and phase informations of the process. Concentrating on the phase differences between the current speed at the 9-m level and those levels below it, and by measuring these differences as deviations in radians from 2π, Fig. 11 clearly demonstrated that the phase

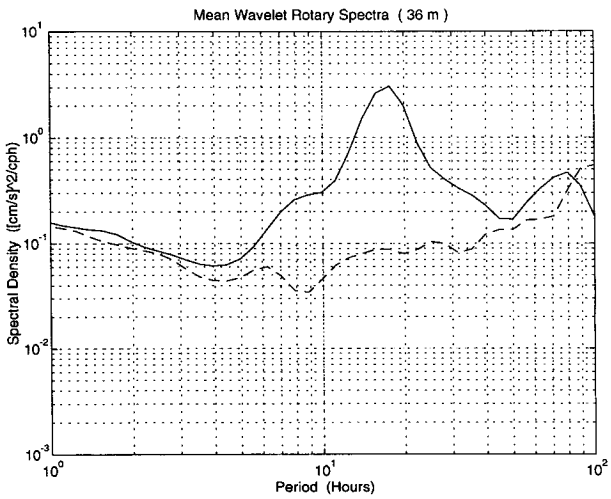

FIG. 8. Mean wavelet rotary spectra at 36-m level. Clockwise and counterclockwise spectra are shown by solid and dashed lines, respectively.

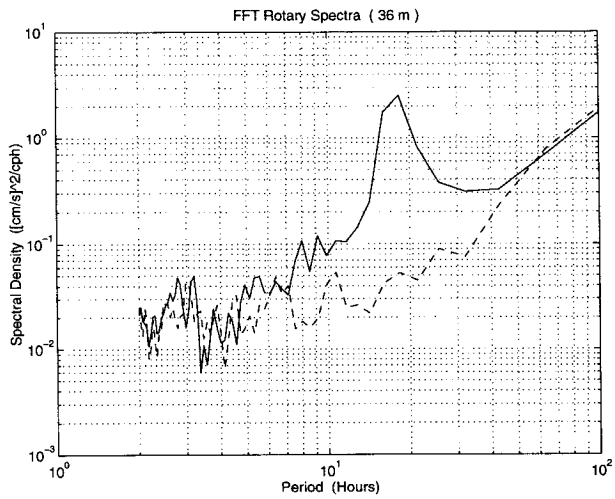

FIG. 9. Conventional FFT rotary spectra at 36-m level. Clockwise and counterclockwise spectra are shown by solid and dashed lines, respectively.

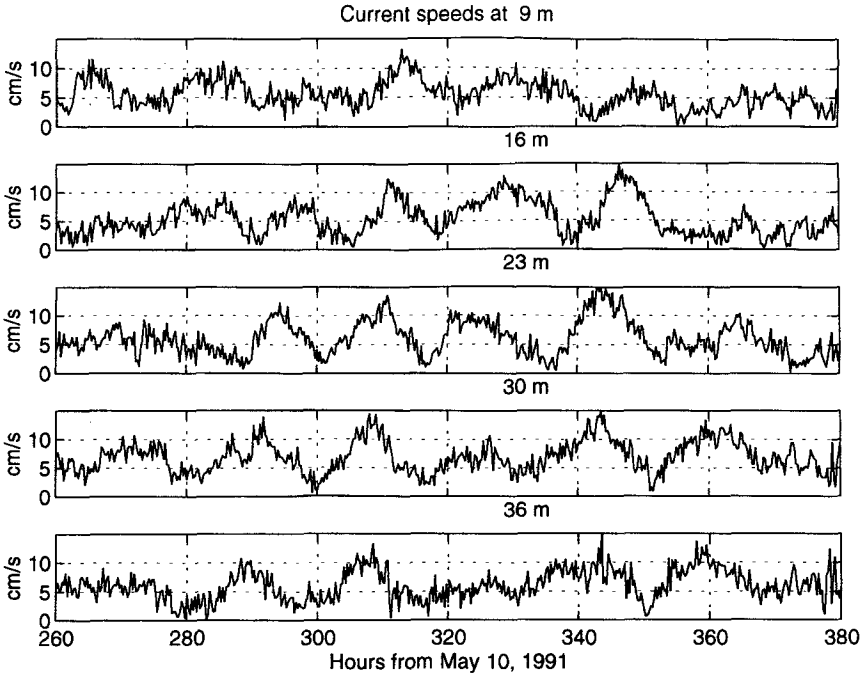

FIG. 10. Time series plots of the current speeds during the inertial motion intensive period.

propagates upward during the same inertial motion intensive period of Fig. 10. This interesting and encouraging result serves to extend the validation on the usefulness of wavelet transform approach.

4. Concluding remarks

An example of applying wavelet transform analysis to the study of current velocity time series data has been presented. Wavelet transform analysis provides the potential to examine the characteristics of the analyzed time series in time and frequency domains rather than in the frequency domain alone using conventional Fourier transform analysis. It is clearly a significant step toward analysis and understanding of current dynamics. There are many important analysis issues that can be addressed with this new and promising approach, both on current analysis and wavelet transform applications. As a first attempt, we have shown the feasibility and usefulness of using the wavelet transform approach. Based on these results, wavelet analysis will probably become part of an essential approach for current data analysis studies.

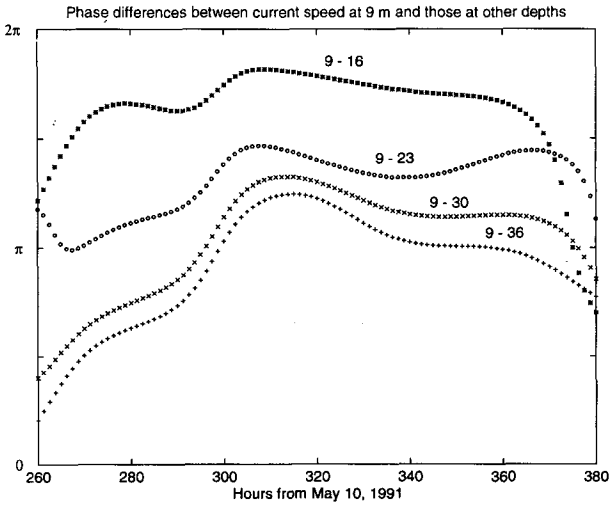

FIG. 11. Phase differences between current speeds at 9 m and those at other depths during the same intensive inertial motion period as shown in Fig. 10.

Acknowledgments. We wish to thank our GLERL colleagues D. J. Schwab and J. H. Saylor for many helpful suggestions and discussions. Thanks also go to the reviewers, especially Dr. C. H. Mortimer, for their constructive comments that have helped to clarify and improve some parts of the paper.

REFERENCES

Combes, J. A., A. Grossmann, and P. Tchamitchian, Eds., 1989: *Wavelets, Time-Frequency Methods and Phase Space.* 2d ed. Springer-Verlag, 315 pp.

Daubechies, I., 1990: The wavelet transform, time-frequency localization and signal analysis. *IEEE Trans. Inf. Theory,* **36,** 961–1005.

Farge, M., 1992: Wavelet transform and their applications to turbulence. *Ann. Rev. Fluid Mech.,* **24,** 395–457.

Gonella, J., 1972: A rotary-component method for analysing meteorological and oceanographic vector time series. *Deep-Sea Res.*, **19,** 833–846.

Konyaev, K. V., 1990: *Spectral Analysis of Physical Oceanographic Data.* National Science Foundation, 200 pp. (First published as *Spektral' nyi Analiz Sluchainykh Okeanologicheskikh Polei,* Gidrometeoizdat Publishers, 1981.)

Leaman, K. D., and T. B. Sanford, 1975: Vertical energy propagation of internal waves: A vector spectral analysis of velocity profiles. *J. Geophys. Res.*, **80,** 1975–1978.

Liu, P. C., 1994: Wavelet spectrum analysis and ocean wind waves. *Wavelets in Geophysics,* E. Foufoula-Georgiou and P. Kumar, Eds., Academic Press, 970–972.

Moll, R., T. Johengen, A. Bratkovich, J. Saylor, L. Meadow, and G. Pernie, 1993: Vernal thermal fronts in large lakes: A case study from Lake Michigan. *Verh. Int. Ver. Theor. Angew. Limnol.*, **25,** 65–68.

Mooers, C. N. K., 1973: A technique for the cross spectrum analysis of pairs of complex valued time series, with emphasis on properties of polarized components and rotational invariants. *Deep-Sea Res.*, **20,** 1129–1141.

Morlet, J., G. Arens, I. Fourgeau, and D. Giard, 1982: Wave propagation and sampling theory. *Geophysics,* **47,** 203–236.

Mortimer, C. H., 1963: Frontiers in physical limnology with particular reference to long waves in rotating basins. *Proc. 6th Conf. Great Lakes Res.*, **9,** 9–42.

——, 1993: Long internal waves in lakes: Review of a century of research. University of Wisconsin–Milwaukee, Center for Great Lakes Studies Special Rep. 42, 117 pp. [Available from Center for Great Lakes Studies, University of Wisconsin–Milwaukee, Milwaukee, WI 53204.]

Rao, D. B., C. H. Mortimer, and D. J. Schwab, 1976: Surface normal modes of Lake Michigan: Calculations compared with spectra of observed water level fluctuations. *J. Phys. Oceanogr.*, **6,** 575–588.

Saylor, J. H., J. C. K. Huang, and R. O. Reid, 1980: Votex modes in southern Lake Michigan. *J. Phys. Oceanogr.*, **10,** 1814–1823.

Weng, H. Y., and K. M. Lau, 1994: Wavelets, period doubling and time-frequency localization with application to organization of convection over the tropical western Pacific. *J. Atmos. Sci.*, **51,** 2523–2541.